DOI: 10.1002/asia.200800074

Robust Tris-Cyclometalated Iridium(III) Phosphors with Ligands for Effective Charge Carrier Injection/Transport: Synthesis, Redox, Photophysical, and Electrophosphorescent Behavior

Guijiang Zhou,[a] Qi Wang,[b] Cheuk-Lam Ho,[a] Wai-Yeung Wong,*[a] Dongge Ma,*[b] Lixiang Wang,[b] and Zhenyang Lin[c]

Abstract: With the target to design and develop new functionalized green triplet light emitters that possess distinctive electronic properties for robust and highly efficient phosphorescent organic light-emitting diodes (PHOLEDs), a series of bluish–green to yellow–green phosphorescent tris-cyclometalated homoleptic iridium(III) complexes [Ir(ppy-X)$_3$] (X = $SiPh_3$, $GePh_3$, NPh_2, $POPh_2$, OPh, SPh, SO_2Ph, Hppy = 2-phenylpyridine) have been synthesized and fully characterized by spectroscopic, redox, and photophysical methods. By chemically manipulating the lowest triplet-state character of Ir(ppy)$_3$ with some functional main-group 14–16 moieties on the phenyl ring of ppy, a new family of metallophosphors with high-emission quantum yields, short triplet-state lifetimes, and good hole-injection/hole-transporting or electron-injection/electron-transporting properties can be obtained. Remarkably, all of these Ir^{III} complexes show outstanding electrophosphorescent performance in multilayer doped devices that surpass that of the state-of-the-art green-emitting dopant Ir(ppy)$_3$. The devices described herein can reach the maximum external quantum efficiency (η_{ext}) of 12.3%, luminance efficiency (η_L) of 50.8 cd A^{-1}, power efficiency (η_p) of 36.9 Lm W^{-1} for [Ir(ppy-$SiPh_3$)$_3$], 13.9%, 60.8 cd A^{-1}, 49.1 Lm W^{-1} for [Ir(ppy-NPh_2)$_3$], and 10.1%, 37.6 cd A^{-1}, 26.1 Lm W^{-1} for [Ir(ppy-SO_2Ph)$_3$]. These results provide a completely new and effective strategy for carrier injection into the electrophosphor to afford high-performance PHOLEDs suitable for various display applications.

Keywords: electron transport · iridium · main group elements · phosphorescence · UV/Vis spectroscopy

Introduction

Owing to their thin-film, high-contrast, light-weight, fast-response, wide-view-angle and low-power attributes, organic light-emitting diodes (OLEDs) have been well recognized in recent years as one of the best flat-panel display technologies that are capable of meeting the most stringent demands of future display applications. This area of research definitely renders OLEDs highly competitive as compared with the now-dominant liquid-crystal displays. So many researchers have continued to devote their efforts to this frontier in both academia and industry since the pioneering work from Kodak in the late eighties.[1] The work generally covers the search for new emissive and host materials within the red–green–blue (RGB) color spectrum, optimization of device structures for electroluminescence (EL) efficiency enhancement, and best operational stabilities.[2] While the EL efficiencies for devices based on the singlet-state fluorescent materials are limited according to spin statistics, organic

[a] Dr. G. Zhou, Dr. C.-L. Ho, Prof. W.-Y. Wong
Department of Chemistry and
Centre for Advanced Luminescence Materials
Hong Kong Baptist University
Waterloo Road, Kowloon Tong, Hong Kong (P.R. China)
Fax: (+852) 3411-7348
E-mail: rwywong@hkbu.edu.hk

[b] Q. Wang, Prof. D. Ma, Prof. L. Wang
State Key Laboratory of Polymer Physics and Chemistry
Changchun Institute of Applied Chemistry
Chinese Academy of Sciences
Changchun 130022 (P.R. China)
Fax: (+86) 431-8526-2873
E-mail: mdg1014@ciac.jl.cn

[c] Prof. Z. Lin
Department of Chemistry
The Hong Kong University of Science and Technology
Clearwater Bay, Hong Kong (P.R. China)

Supporting information for this article is available on the WWW under http://dx.doi.org/10.1002/asia.200800074.

WILEY InterScience DISCOVER SOMETHING GREAT
© 2008 Wiley-VCH Verlag GmbH & Co. KGaA, Weinheim

phosphorescent metal complexes of heavy transition metals, especially the cyclometalated iridium(III) congeners, provide a major breakthrough in the advancement of high-efficiency phosphorescent OLEDs (PHOLEDs) as they can harness both singlet and triplet excitons in the emission process.[3]

Generally speaking, it was not until the discovery of metalated phosphorophores that researchers began intensive investigations on white OLEDs (WOLEDs) as a practical avenue towards thin-film solid-state lighting sources. For example, the power efficiency should be about 10–15 Lm W^{-1} for a conventional white-light incandescent lamp and a power efficiency of 70 Lm W^{-1} is required for a tube fluorescent lamp.[4] As a result, the development of highly efficient organic phosphors of various colors becomes crucial for the eventual success of WOLEDs. White-light emission can be obtained by mixing three primary colors (R–G–B) in a multi- or a single-layer structure from small molecules and/or polymers.[4e,f,m,n] More recently, two-color systems involving complementary blue and orange or red light-emitters can be employed to obtain a wide EL spectrum to mimic the white light spectrum.[4i,5] Many reported WOLEDs with dual emission layers typically display an obvious valley in the green-light region of their EL spectra,[4h,k,6] indicating their poor color rendering index (CRI) especially for green-colored objects viewed in white light. Although such a drawback can, in some instances, be partially tackled using the emission tail from the blue-emitting component, a proper green light emission would be highly beneficial for many practical applications. So, a green-emitting layer consisting of $Ir(ppy)_3$ (Hppy = 2-phenylpyridine) doped in a suitable host was commonly inserted in WOLEDs to effectively compensate for the green-light deficiency in the EL spectra in order to obtain a better white-light chromaticity. These devices usually show a more desirable white EL spectrum with a high CRI.[6] Currently, much less attention has been paid to the development of new green-emitting Ir^{III}-based phosphors relative to their blue[7] and orange/red[8] counterparts. Although there are numerous reports over the years on using the benchmark $Ir(ppy)_3$ green emitter in the PHOLED field,[3b,9] relevant work on the facile functionalization of green triplet emitters featuring specific charge carrier injection and transport character is still highly desirable and challenging.[10,11] Some recent examples include the work on Ir^{III} complexes with a dendritic skeleton or those with hole-injection/hole-transporting (HI/HT) moieties.[11]

Abstract in Chinese:

本文设计合成了一系列以 14 至 16 主族元素基团功能化的高性能 2-苯基吡啶铱类三线态发光材料。利用所采用主族元素基团所固有的电子特性，成功地赋予这类新颖的发光材料良好的电子及空穴 的注入及传输性能。因此这些绿色发光材料表现出优异的电致发光性能：最大外量子效率可达 13.9%；最大电流效率可达 60.8 cd A^{-1}；最大功率效率为 49.1 lm W^{-1}。所有这些结果表明这一设计思想对于设计合成用于各种显示技术的三线态发光材料具有重要意义。

However, to our knowledge, Ir^{III} phosphors with electron-injection/electron-transporting moieties (EI/ET), which are equally vital for an improved balance in charge injection and transport, are very scarce.[10f] It is well accepted that nonmetallic main-group elements show distinct electronic features according to their intrinsic nature. Furthermore, the electronic character of some elements in these main groups, such as P and S and so forth, can be altered dramatically by suitable chemical modifications. So, we would expect to observe unique electronic properties for Ir^{III} complexes by integrating these main-group moieties into the ligand frameworks of these metallophosphors. Hence, we describe herein an interesting series of small-molecule green-emitting Ir^{III} phosphors showing diverse electronic properties. Among these complexes, the phenyl ring of ppy has been derivatized by various distinctive main-group 14–16 moieties and their excellent EL performance set them apart as very promising green-emitting phosphorescent candidates for high-quality green PHOLEDs and possibly for WOLEDs. Some of these complexes also represent the first examples of metallophosphors with promising EI/ET properties.

Results and Discussion

Synthesis, Structural Characterization, and Theoretical Calculations

Chemical structures and the synthetic protocols of the new Ir^{III} complexes $[Ir(ppy\text{-}X)_3]$ (X = $SiPh_3$, $GePh_3$, NPh_2, $POPh_2$, OPh, SPh, SO_2Ph) are shown in Scheme 1. As the key compounds, the organic cyclometalating ligands were conveniently prepared by Stille coupling of 2-(tributylstannyl)pyridine with the appropriate main-group element-bridged aryl halides (see Scheme S1 in the Supporting Information). All of the homoleptic complexes were synthesized in a single step from the cyclometalation of $[Ir(acac)_3]$ (acac = acetylacetonate) with the corresponding organic ligand in glycerol at approximately 230 °C.[3g] These air-stable compounds were isolated in high purity as pale yellow to orange-yellow solids by column chromatography on silica gel with the proper eluent.

All of the Ir compounds were fully characterized by NMR spectroscopy and fast-atom-bombardment mass spectrometry (FAB-MS). ^1H and ^{13}C NMR data suggested that the stereochemistry of these triply cyclometalated complexes is that of facial isomers with inherent C_3 symmetry because the NMR chemical shifts observed in the three ligands were equivalent. In each case, the FAB-MS spectrum reveals the respective parent-ion peak clearly. Presumably owing to the amorphous nature of these compounds, so far, all attempts to get single crystals have met with little success except for **Ir-SO_2**. The X-ray crystal structure of **Ir-SO_2** reveals the central Ir cation to be coordinated by three anionic C^N ligands. The coordination around the Ir center consists of the *fac*-$Ir(C^N)_3$ chelate disposition arranged in a distorted octahedron (Table 1, Figure 1 and Table S1 in the Supporting Information).

 © 2008 Wiley-VCH Verlag GmbH & Co. KGaA, Weinheim

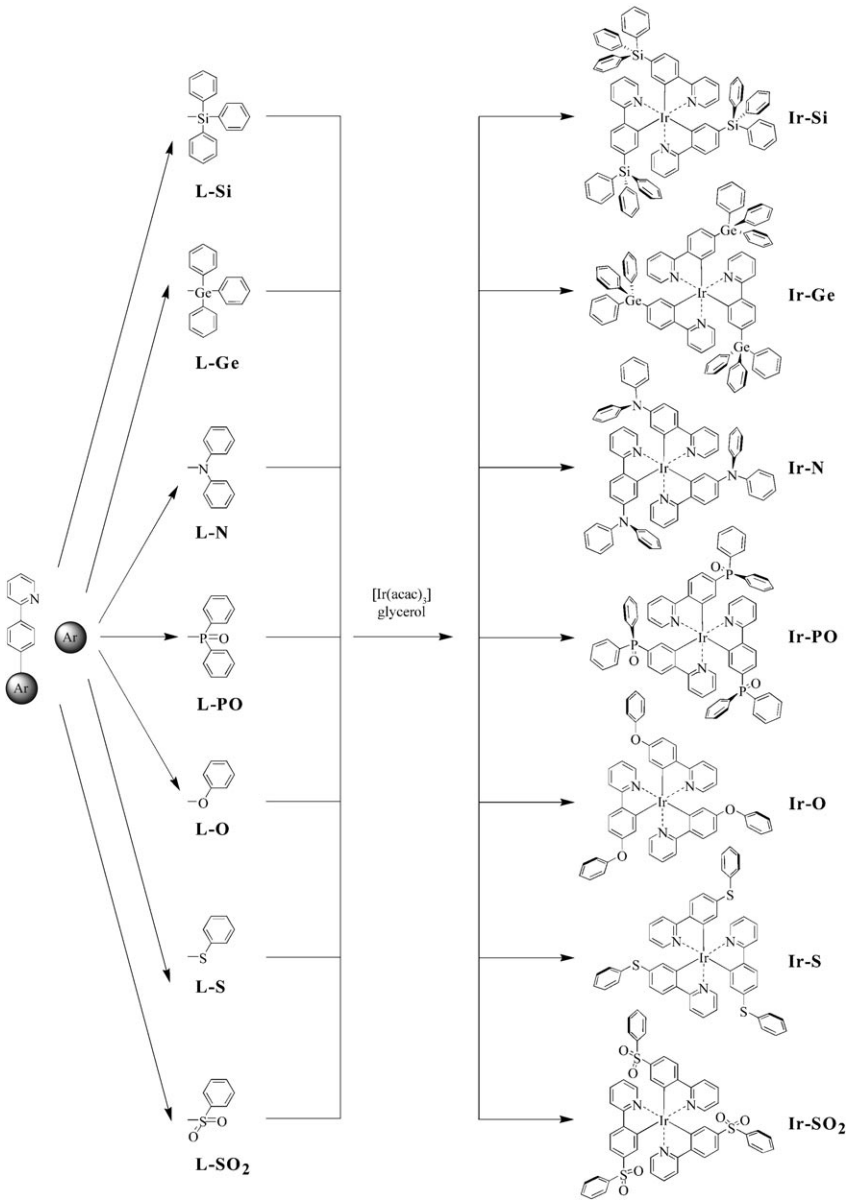

Scheme 1. Synthesis of new phosphorescent homoleptic iridium(III) complexes.

Table 1. Selected structural parameters for **Ir-SO$_2$**.

Bond Angles [°]					
N(2)-Ir(1)-C(28)		79.39(10)	C(45)-Ir(1)-N(2)		91.63(9)
C(28)-Ir(1)-C(11)		94.24(10)	C(45)-Ir(1)-C(28)		94.49(10)
C(11)-Ir(1)-N(3)		89.68(9)	C(45)-Ir(1)-C(11)		94.83(10)
N(3)-Ir(1)-N(2)		97.29(9)	C(45)-Ir(1)-N(3)		79.28(9)
N(1)-Ir(1)-N(2)		94.42(9)	N(2)-Ir(1)-C(11)		171.28(9)
N(1)-Ir(1)-C(28)		90.65(9)	C(28)-Ir(1)-N(3)		172.92(8)
N(1)-Ir(1)-C(11)		79.59(9)	N(1)-Ir(1)-C(45)		172.69(9)
N(1)-Ir(1)-N(3)		95.87(8)			
Bond Lengths [Å]					
Ir(1)–N(1)	2.135(2)	Ir(1)–N(2)	2.114(2)	Ir(1)–N(3)	2.127(2)
Ir(1)–C(11)	2.006(2)	Ir(1)–C(28)	2.011(3)	Ir(1)–C(45)	2.002(2)

The X-ray crystallographic results also provide valuable structural information for the computational studies of the ground-state electronic properties of the molecule, which has a close relationship with the photophysical behavior. Based on the crystal data of **Ir-SO$_2$**, its frontier orbital patterns were obtained by theoretical computations, using the density functional theory (DFT) method (Figure 2). The highest occupied molecular orbital (HOMO) of **Ir-SO$_2$** is mainly located on the t_{2g}-d orbitals of the iridium center (approximately 51.4%), while the main contribution to the lowest unoccupied molecular orbital (LUMO) comes from the π-orbitals of the pyridyl ring in the cyclometalating ligands. Furthermore, our time-dependent density functional theory (TD-DFT) calculations show that the $S_1 \leftarrow S_0$ transitions correspond to the HOMO→LUMO transitions with a non-zero oscillator strength of 0.007 for the transition (see Table S2 in the Supporting Information). So the lowest excited state in **Ir-SO$_2$** shows strong metal-to-ligand charge transfer (MLCT) character.

Thermal and Photophysical Properties

The thermal properties of these new Ir^{III} complexes were studied by thermogravimetric analysis (TGA) and differential scanning calorimetry (DSC) under a nitrogen atmosphere (Table 2). The main-group moieties such as arylsilanes are expected to provide high thermal and chemical stability as well as glassy properties when incorporated into the $Ir(ppy)_3$ core.[13] The TGA results reveal excellent thermal stability of the complexes and their 5% weight-loss temperatures ($\Delta T_{5\%}$) range from 384 to 487 °C. This data renders the materials suitable for the fabrication of PHOLEDs by using the vacuum thermal deposition method. The slightly lower thermal stability of **Ir-S** in the series might be ascribed to the electron-rich nature of the sulfur atom towards oxidative reactions. Thermally induced phase-transition behavior of the molecules was also investigated with DSC technology.

 © 2008 Wiley-VCH Verlag GmbH & Co. KGaA, Weinheim

CHEMISTRY
AN ASIAN JOURNAL

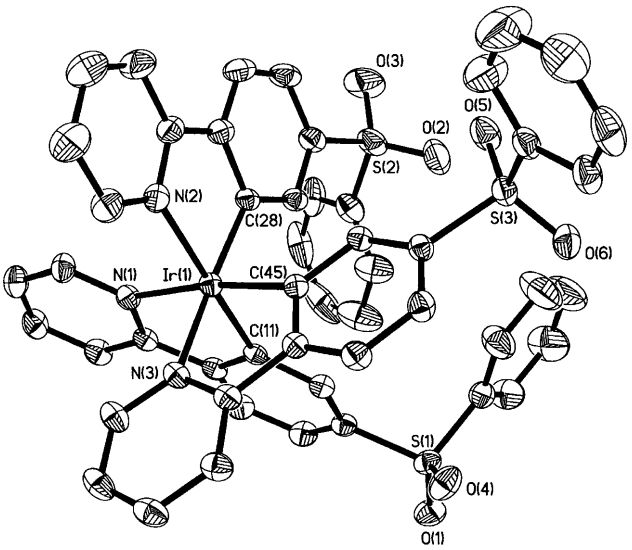

Figure 1. An ORTEP drawing of **Ir-SO$_2$** with thermal ellipsoids drawn at 25% probability level. Labels on the carbon atoms (except for those bonded to Ir) and hydrogen atoms are omitted for clarity.

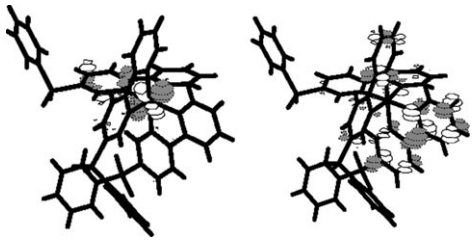

Figure 2. Plots of the HOMO (left) and LUMO (right) for **Ir-SO$_2$**.

DSC traces for all of the complexes showed no crystallization or melting processes but only glass-transition behavior. Each of them showed a very high glass-transition temperature (T_g) in excess of 157 °C and their highly amorphous nature in the solid state can be attributed to the branched and twisted configuration of the substituted main-group moieties despite the relatively small ligand size of the complexes. This favorable feature would afford new Ir^{III} complexes with improved compatibility between the phosphor dopant and the organic small-molecule host for high-efficiency PHOLED performance.

As shown in Figure 3a (see also Figure S2 in the Supporting Information), the UV/Vis spectra of the [Ir(ppy-X)$_3$] series exhibit two major absorption bands. The intense UV bands ($\log\varepsilon > 4.0$) are assigned to the spin-allowed $S_1 \leftarrow S_0$ transitions of the organic chromophores (i.e. π–π* bands),

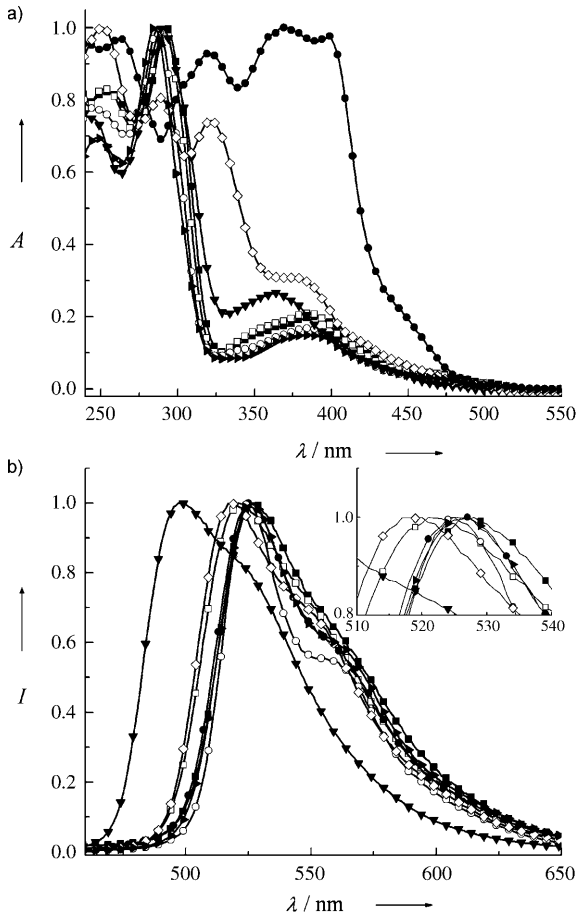

Figure 3. a) UV/Vis and b) PL spectra of the iridium complexes in CH_2Cl_2 at 293 K. ■: **Ir-Si**, □: **Ir-Ge**, ●: **Ir-N**, ○: **Ir-PO**, ▼: **Ir-O**, ◇: **Ir-S**, ▶: **Ir-SO$_2$**.

Table 2. Photophysical and thermal-stability data for the new homoleptic Ir^{III} complexes.

Compound	Absorption (293 K) λ_{abs} [nm][a]	Emission λ_{em} [nm] 293 K/77 K	Φ_p[b]	τ_p [μs][c]	τ_r [μs][d]	k_r [s^{-1}]	k_{nr} [s^{-1}]	$\Delta T_{5\%}/T_g$ [°C][e]
Ir-Si	255 (4.65), 293 (4.73), 388 (4.03), 465 (3.41), 502 (2.94)	530/527	0.48	0.11	0.23	4.4×10^6	4.7×10^6	447/165
Ir-Ge	253 (4.69), 291 (4.76), 388 (4.07), 465 (3.40), 502 (2.75)	525/521	0.53	0.11	0.21	4.8×10^6	4.3×10^6	435/163
Ir-N	262 (4.76), 269 (4.72), 320 (4.56), 367 (4.60), 399 (4.58), 450 (3.87)	528/526	0.13	0.10	0.77	1.3×10^6	8.7×10^6	450/157
Ir-PO	247 (4.66), 287 (4.71), 384 (3.95), 471 (3.22), 503 (2.83)	525/527	0.70	0.18	0.26	3.9×10^6	1.7×10^6	451/183
Ir-O	243 (4.65), 290 (4.77), 364 (4.09), 400 (3.97), 476 (2.83)	497/494	0.57	0.10	0.18	5.7×10^6	4.3×10^6	441/166
Ir-S	251 (4.76), 289 (4.67), 322 (4.63), 376 (4.25), 423 (3.86), 499 (2.70)	520/517	0.42	0.15	0.34	2.8×10^6	3.9×10^6	384/161
Ir-SO$_2$	247 (4.66), 285 (4.81), 388 (4.00), 473 (3.26), 506 (2.57)	527/532	0.91	0.25	0.27	3.6×10^6	3.6×10^6	487/170

[a] Measured in CH_2Cl_2 at a concentration of 10^{-5} M and $\log\varepsilon$ values are shown in parentheses. sh = shoulder. [b] In degassed CH_2Cl_2 relative to *fac*-[Ir(ppy)$_3$] ($\Phi_p = 0.40$), $\lambda_{ex} = 360$ nm. [c] Measured in freeze–pump–thaw degassed CH_2Cl_2 solutions at a sample concentration of approximately 10^{-5} M and the excitation wavelength was set at 355 nm for all of the samples at 293 K. [d] The triplet radiative lifetimes were deduced from $\tau_r = \tau_P/\Phi_P$. [e] $\Delta T_{5\%}$ is the 5% weight-loss temperature and T_g is the glass transition temperature.

 © 2008 Wiley-VCH Verlag GmbH & Co. KGaA, Weinheim

which are located below 300 nm for all of the complexes except for **Ir-N** and **Ir-S**. The latter two complexes show the $S_1 \leftarrow S_0$ transitions at much lower energies (approximately 322 nm for **Ir-S** and 399 nm for **Ir-N**), attributable to the strongly electron-donating properties of the attached main-group moieties. The weaker, low-energy features for these Ir^{III} complexes result from both $^1MLCT \leftarrow S_0$ and $^3MLCT \leftarrow S_0$ transitions. The oscillator strength of $^3MLCT \leftarrow S_0$ transition is close to that of the lower-energy featured $^1MLCT \leftarrow S_0$ (less than a factor of two in their extinction coefficients for the two MLCT bands (Table 2)),[3g,15b] indicating that the $^3MLCT \leftarrow S_0$ transition is strongly allowed by a significant singlet-triplet state mixing owing to the spin-orbit coupling induced by the heavy Ir metal. Although each of the compounds **Ir-Si**, **Ir-Ge**, **Ir-PO**, and **Ir-SO_2** gives a similar major $^1MLCT \leftarrow S_0$ transition band centered at approximately 390 nm, there is a slight bathochromic shift for the weaker $^3MLCT \leftarrow S_0$ transition for **Ir-PO** and **Ir-SO_2** as compared with that of **Ir-Si** and **Ir-Ge**. As the S atom is more polarizable than the O atom, this would result in an enhanced conjugative effect[14] and therefore **Ir-S** shows a red shift in both $^1MLCT \leftarrow S_0$ and $^3MLCT \leftarrow S_0$ transition bands with reference to those from **Ir-O. Ir-N** shows the MLCT band at the lowest energies (as a shoulder at approximately 450 nm), which can be rationalized from the fact that the strongly electron-donating NPh_2 substituent in **Ir-N** destabilizes the HOMO level by the mesomeric effect.

Under UV light irradiation at 360 nm, all of the homoleptic Ir complexes emit intense bluish-green to yellow-green phosphorescence. The spectra of $[Ir(ppy\text{-}X)_3]$ and $Ir(ppy)_3$ have virtually identical shapes, indicating that the same excited and/or ground states were involved in the phosphorescent transitions. The structureless pattern of the photoluminescence (PL) spectra is suggestive of their predominantly MLCT character for the lowest excited triplet states in these complexes at 293 K (Figure 3b), which is also confirmed by the DFT results (Figure 2). Relative to the parent complex $Ir(ppy)_3$ ($\lambda_{em} \sim 510$ nm), it is obvious that **Ir-N** exhibits a longer emission wavelength (approximately 528 nm) as it contains the cyclometalating ligands anchored with NPh_2 groups, which can push up the HOMO energy by electron donation. Consistent with the absorption features, the emission band of **Ir-S** is bathochromically shifted from **Ir-O** (approximately 520 nm versus 497 nm for **Ir-O**) owing to the lower MLCT energy states of **Ir-S** than **Ir-O**. The OPh moiety, with little participation expected in both the HOMOs and LUMOs in **Ir-O**, cannot offer a good electron sink for the stabilization of MLCT states, thus raising the LUMO level through its inherent good π-donating ability with the phenyl ring to which it is attached, and causing a blue-shift in emission for **Ir-O** relative to $Ir(ppy)_3$. For the four phosphors **Ir-Si**, **Ir-Ge**, **Ir-PO**, and **Ir-SO_2**, they also show emission maxima in the green region (525–530 nm), signaling their close MLCT energy states. However, we note that there are different mechanisms for the red shifts in the MLCT emission energies among the complexes in the series as compared with that of $Ir(ppy)_3$. According to the traditional color-tuning strategy reported in the literature,[15] the emission maximum of an Ir^{III} cyclometalated complex typically shows a hypsochromic shift when an electron-withdrawing group (such as F) is introduced to the phenyl ring of ppy. In contrast, our new complexes **Ir-PO** and **Ir-SO_2**, each consisting of an electron-withdrawing group on the phenylpyridine moiety, display the opposite trend and emit at longer wavelengths of approximately 525 and 527 nm, respectively, than $Ir(ppy)_3$. It is our contention that the inductively electron-withdrawing $POPh_2$ and SO_2Ph moieties can somehow act as the destination for electrons in the MLCT processes and stabilize the MLCT states accordingly. The way **Ir-SO_2** behaves is quite similar to that observed in some pentafluorophenyl-substituted Ir complexes in which the incorporation of an electron-withdrawing pentafluorophenyl group to the ppy ring and the position of substitution can be used to tune the emission color.[10f] Consistent with previous observations on some aromatic systems with $POPh_2$ moieties,[16] the strong inductive-withdrawing influence of the polar P=O group in **Ir-PO** was shown to significantly lower the LUMO energy, thus red shifting the emission relative to $Ir(ppy)_3$. Saliently, we present herein an interesting color-tuning method in Ir^{III} complexes, which contrasts with the well-documented protocols. The apparent π-accepting abilities of $SiPh_3$ and $GePh_3$ are mainly responsible for the longer emission wavelengths for **Ir-Si** and **Ir-Ge** (approximately 530 and 525 nm, respectively) than $Ir(ppy)_3$. Arising from the weaker π-bonding ability of the O atoms in the acetylacetonate ($acac^-$) ligand compared with ppy,[17] this new color-tuning venture would be expected to be even more effective for the corresponding heteroleptic series $[Ir(ppy\text{-}X)_2(acac)]$.[11f]

The phosphorescent quantum yields (Φ_p) for all of the new triplet emitters were also measured in CH_2Cl_2 against the $Ir(ppy)_3$ standard (Table 2). Most of them show high Φ_p (0.42–0.57 for **Ir-Si**, **Ir-Ge**, **Ir-O**, and **Ir-S**; 0.70–0.91 for **Ir-PO** and **Ir-SO_2**), which are probably attributed to the branched and dendritic architecture that can shield the emission center against undesirable nonradiative pathways. The exceptionally high Φ_p values for **Ir-PO** and **Ir-SO_2** might be attributed to the presence of electron-withdrawing groups that can facilitate the formation of MLCT states in both complexes. This clearly demonstrates the merit of introducing electron-withdrawing moieties to the $Ir(ppy)_3$ emissive core to afford the highly efficient phosphorescent Ir complexes that are desirable for high-performance PHOLEDs. The observed phosphorescence lifetimes, τ_P, have a magnitude of about 0.10–0.25 μs, which are much shorter than that of the reference compound $Ir(ppy)_3$ ($\tau_P \sim 0.5$ μs). It is widely accepted that a longer lifetime of a phosphorescent emitter would cause severe triplet–triplet annihilation, especially at high current density. Thus, this detrimental issue in many PHOLEDs is likely to be relieved with the inclusion of these main-group moieties. Accordingly, the radiative lifetimes (τ_r) of the triplet excited state deduced from $\tau_r = \tau_P/\Phi_P$ are as short as 0.18–0.77 μs,[3f] which correlates well with the

 © 2008 Wiley-VCH Verlag GmbH & Co. KGaA, Weinheim

unusually large extinction coefficients of the ^{3}MLCT bands. The triplet radiative and nonradiative rate constants, k_r and k_{nr}, can be derived from Φ_P and τ_P using the relationships $\Phi_P = \Phi_{ISC}\{k_r/(k_r + k_{nr})\}$ and $\tau_P = (k_r + k_{nr})^{-1}$. Here, Φ_{ISC} is the intersystem-crossing yield which can be safely assumed to be 1.0 for iridium complexes because of the strong spin–orbit coupling interaction caused by the heavy-atom effect of iridium. It is found that the k_r value, in the order of $10^6\ s^{-1}$ for our [Ir(ppy-X)$_3$] complexes, is larger than that found for Ir(ppy)$_3$ ($8.0\times10^5\ s^{-1}$). This would be advantageous to the molecular design of highly efficient devices based on light-energy harvesting from the triplet excitons.

All of the Ir^{III} complexes are also strongly phosphorescent in glass matrices at 77 K (Figure S3 in the Supporting Information). Typical of other similar Ir^{III} complexes,[4b] the PL spectra display more structured spectral profiles upon cooling the solutions to 77 K, which suggest the involvement of some ligand-centered character.

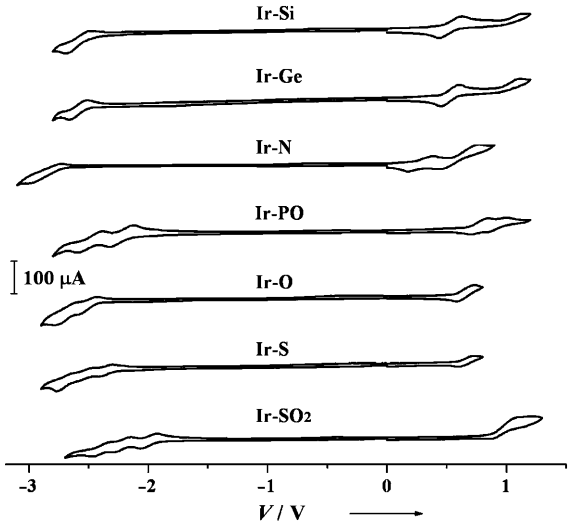

Figure 4. Cyclic voltammograms for the seven iridium(III) complexes.

Redox Properties

The electrochemical properties of our materials were investigated by cyclic voltammetry (CV) by using ferrocene as the internal standard. The results are listed in Table 3 and presented in Figure 4. The Ir complexes with main-group 14 moieties **Ir-Si** and **Ir-Ge** show very similar redox behavior ($E_{1/2}^{ox}$ 0.23 and 0.24 V; $E_{1/2}^{red}$ −2.88 V), rendering them with very similar HOMO and LUMO levels. As compared with the data of Ir(ppy)$_3$ measured under identical experimental conditions (HOMO −5.08 eV and LUMO −1.91 eV, close to the reported data[18]), the addition of the main-group 14 moieties would not influence the energy of the LUMO level much but the HOMO energy is slightly elevated owing to the larger π-conjugation length of their ligands relative to the neat ppy. Although it is known that the aromatic silyl systems can show high-electron-affinity properties to some extent,[19] the reduction wave in the CV scan of **Ir-Si** and **Ir-Ge** should be assigned to the reduction of the strongly electron-deficient pyridyl moiety in their ligands as **Ir-Si** and **Ir-Ge** show almost the same LUMOs to that of Ir(ppy)$_3$. Owing to the addition of electron-rich diphenylamino groups, **Ir-N** is much easier to be oxidized ($E_{1/2}^{ox}$ 0.15 V) and shows an elevated HOMO level (approximately −4.95 eV) relative to Ir(ppy)$_3$, which will facilitate the hole injection to the complex. The electron-rich ligand also makes **Ir-N** much more difficult to be reduced ($E_{1/2}^{red}$ −2.99 V), leading to a much higher LUMO (approximately −1.81 eV). With the inductively electron-withdrawing $POPh_2$ and SO_2Ph moieties, **Ir-PO** and **Ir-SO$_2$** are readily reduced and give the first $E_{1/2}^{red}$ of −2.56 and −2.32 V, respectively, which should be ascribed to the reduction of $POPh_2$ and SO_2Ph. Compared with that of Ir(ppy)$_3$ ($E_{1/2}^{red}$ −2.89 V), the higher reduction potentials for **Ir-PO** and **Ir-SO$_2$** indicate their lower LUMO energies (−2.24 eV for **Ir-PO** and −2.48 eV for **Ir-SO$_2$**; Figure 4), favoring the EI/ET character. Therefore, **Ir-PO** and **Ir-SO$_2$** provide the first examples of green-emitting Ir^{III} phosphors with promising EI/ET features. The other reduction waves at the more negative potentials for **Ir-PO** and **Ir-SO$_2$** are owing to the reduction of the pyridyl ring. Likewise, **Ir-PO** and **Ir-SO$_2$** are more difficult to be oxidized as compared with Ir(ppy)$_3$ and related derivatives. They have higher oxidation potentials ($E_{1/2}^{ox}$ 0.45 V and 0.65 V, respectively), which would not promote HI/HT. In general, the HI/HT feature is quite common in iridium complexes as many of them possess π-conjugated organic ligands, which would make the EI/ET unlikely. As a result, the relatively poorer HI/HT properties of **Ir-PO** and **Ir-SO$_2$** together with their good potentials in EI/ET would offer a more balanced carrier injection to **Ir-PO** and **Ir-SO$_2$**, which would be an added advantage to the overall performance of PHOLEDs prepared with these two emitters. **Ir-O** and **Ir-S**, possessing main-group 16 moieties, show almost identical first oxidation potentials, but **Ir-S** gives a lower LUMO level. **Ir-S**, with a smaller HOMO–LUMO gap, gives a longer emission wavelength than **Ir-O** (Table 2). All of the oxidation and reduction processes of the complexes are quasi-reversible and such a good reversibility in their electrochemical behavior will be beneficial to the overall stability of the PHOLEDs based on these Ir dopants.

Table 3. Redox properties of the new iridium(III) complexes.

Compound	$E_{1/2}^{ox}$ [V]	$E_{1/2}^{red}$ [V]	HOMO [eV]	LUMO [eV]
Ir-Si	0.23	−2.88	−5.03	−1.92
Ir-Ge	0.24	−2.88	−5.04	−1.92
Ir-N	0.15, 0.47	−2.99	−4.95	−1.81
Ir-PO	0.45, 0.59	−2.56, −2.82	−5.25	−2.24
Ir-O	0.35	−2.83, −3.01	−5.15	−1.97
Ir-S	0.35	−2.68, −2.86, −3.02	−5.15	−2.12
Ir-SO$_2$	0.65, 0.85	−2.32, −2.55, −2.72	−5.45	−2.48
Ir(ppy)$_3$	0.28	−2.89	−5.08	−1.91

© 2008 Wiley-VCH Verlag GmbH & Co. KGaA, Weinheim

Fabrication and Characterization of PHOLEDs

All of the Ir^{III} complexes readily sublime under vacuum, which should be amenable to thermally evaporated OLED device fabrication. Inspired by the high Φ_P and good carrier-injection or -transporting (i.e., EI/ET and HI/HT) properties of these triplet emitters, we have prepared doped PHOLEDs by the high-vacuum deposition method. Figure 5 depicts the general structures for the electrophosphorescent devices and the molecular structures of the compounds employed. Owing to its ambipolar charge-carrier-transporting properties and suitable triplet level, 4,4′-*N*,*N*′-dicarbazolebiphenyl (CBP) is used as the carrier combination host for our phosphors. 4,4′-Bis[*N*-(1-naphthyl)-*N*-phenylamino]biphenyl (NPB) serves as a hole-transport layer, 2,9-dimethyl-4,7-diphenyl-1,10-phenanthroline (BCP) as a hole-blocker, tris(8-hydroxyquinolinato)aluminum (Alq_3) as an electron transporter, and LiF as an electron-injection layer. All of the devices consist of the multilayer configuration ITO/NPB (40 nm)/x% Ir:CBP (20 nm)/BCP (10 nm)/Alq_3 (30 nm)/LiF:Al (1:100 nm). To optimize the device efficiency, concentration-dependence experiments were carried out in the range of 4–10 wt%. All of the devices give intense bluish–green to yellow–green EL spectra. The close resemblance of the EL spectra with the PL spectra in each case indicates that the EL originates from the triplet states of the phosphor (Figure 6). None of the EL spectra displayed excimer emission at longer wavelengths, revealing that the main-group substituents in [Ir(ppy-X)$_3$] frustrated the inter-chromophoric interactions at all of the doping ratios tested. No obvious emission from CBP or Alq_3 is visible from each device even at high current densities, which suggests an efficient energy transfer from the host exciton to the phosphor molecule upon electrical excitation and the effective hole-blocking effect of BCP. Table 4 summarizes some EL data for the devices at various phosphor-doping levels (also see Table S3 in the Supporting Information). The devices A1–A4 and B1–B4 prepared from **Ir-Si** and **Ir-Ge** show comparable device performance. Device A2 at the 6 wt% **Ir-Si** doping level gives the peak EL performance with a low turn-on voltage ($V_{turn\,on}$) of 3.9 V, a maximum brightness (L_{max}) of 48333 cd m^{-2} at 15.3 V, a peak external quantum efficiency (η_{ext}) of 12.3%, a luminance efficiency (η_L) of 50.8 cd A^{-1}, and a power efficiency (η_p) of 36.9 Lm W^{-1}. With a similar EL capacity to that of device A2, device B3 at the 8 wt% **Ir-Ge** doping level shows the highest EL efficiencies of 13.4%, 48.4 cd A^{-1}, and 32.6 Lm W^{-1}. This device turns on at 3.9 V and its light output can reach 48567 cd m^{-2} at 14.1 V. The high EL efficiencies can reasonably be correlated to the sufficient steric hindrance of the triphenyl silyl and triphenyl germyl groups to protect typical reactive centers. The device C3 prepared from **Ir-N** (8 wt%) with HI/HT character shows an even more attractive performance (η_{ext} of 13.9%, η_L of 60.8 cd A^{-1}, η_p of 49.1 Lm W^{-1}, L_{max} of 48576 cd m^{-2} at 12.3 V, and $V_{turn\,on}$ of 3.3 V). We observe that the devices F1–F4 doped with **Ir-S** show a much better EL performance than that of devices E1–E4 based on **Ir-O**. For **Ir-S**, device F3 gives the best EL data as indicated by η_{ext} of 12.5%, η_L of 45.9 cd A^{-1}, η_p of 35.0 Lm W^{-1}, L_{max} of 48318 cd m^{-2} at 12.1 V, and $V_{turn\,on}$ of 3.5 V. Device E3 turns on at 3.9 V but it only exhibits η_{ext} of 8.9%, η_L of 26.6 cd A^{-1}, η_p of 18.1 Lm W^{-1}, and L_{max} of 38561 cd m^{-2} at 14.7 V. Electrophosphors featuring EI/ET functions (**Ir-PO** and **Ir-SO$_2$**) can also afford devices with encouraging performance, presumably because they can somehow balance the electrons with the greater number of holes in the host. Device D2 (6 wt% **Ir-PO**) can still show the peak EL efficiencies at η_{ext} of 9.7%, η_L of 34.2 cd A^{-1}, η_p of 23.6 Lm W^{-1},

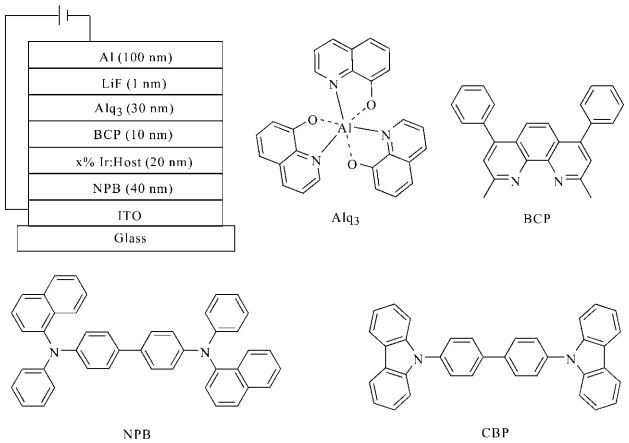

Dopant	Devices and doping level
Ir-Si	**A1** (4 wt%), **A2** (6 wt%), **A3** (8 wt%), **A4** (10 wt%)
Ir-Ge	**B1** (4 wt%), **B2** (6 wt%), **B3** (8 wt%), **B4** (10 wt%)
Ir-N	**C1** (4 wt%), **C2** (6 wt%), **C3** (8 wt%), **C4** (10 wt%)
Ir-PO	**D1** (4 wt%), **D2** (6 wt%), **D3** (8 wt%), **D4** (10 wt%)
Ir-O	**E1** (4 wt%), **E2** (6 wt%), **E3** (8 wt%), **E4** (10 wt%)
Ir-S	**F1** (4 wt%), **F2** (6 wt%), **F3** (8 wt%), **F4** (10 wt%)
Ir-SO$_2$	**G1** (4 wt%), **G2** (6 wt%), **G3** (8 wt%), **G4** (10 wt%)

Figure 5. The general configuration for the electrophosphorescent OLED devices and the molecular structures of the relevant compounds used in these devices.

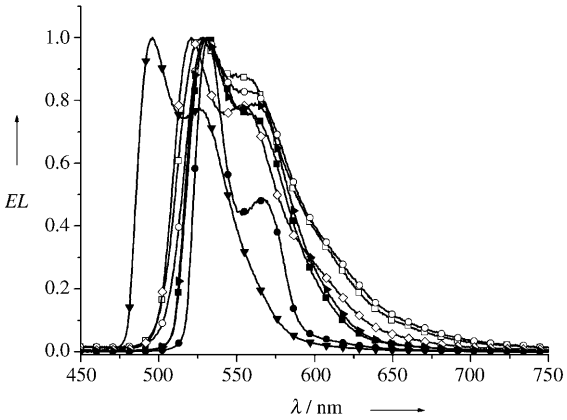

Figure 6. EL spectra for some of the best devices at 8 V. ■: Device A2, □: Device B3, ●: Device C3, ○: Device D2, ▼: Device E3, ◇: Device F3, ▶: Device G2.

 © 2008 Wiley-VCH Verlag GmbH & Co. KGaA, Weinheim

Table 4. The EL performance of the PHOLEDs based on $[Ir(ppy\text{-}X)_3]$.[a]

Device	Phosphor dopant	$V_{turn\,on}$ [V]	Luminance L [cd m^{-2}][b]	η_{ext} [%][b]	η_L [cd A^{-1}][b]	η_p [Lm W^{-1}][b]	λ_{max} [nm][c]
A1	**Ir-Si** (4 wt%)	3.9	48312 (14.9)	9.80 (7.1)	40.60 (7.1)	18.98 (5.1)	531 (0.36, 0.60)
A2	**Ir-Si** (6 wt%)	3.9	48333 (15.3)	12.26 (4.9)	50.79 (4.9)	36.93 (4.1)	531 (0.36, 0.60)
A3	**Ir-Si** (8 wt%)	4.1	48554 (14.9)	11.22 (5.5)	46.49 (5.5)	28.51 (4.9)	531 (0.36, 0.60)
A4	**Ir-Si** (10 wt%)	3.9	48290 (15.3)	10.77 (4.9)	44.62 (4.9)	29.87 (4.5)	531 (0.36, 0.60)
B1	**Ir-Ge** (4 wt%)	4.1	48530 (14.3)	10.06 (4.9)	36.47 (4.9)	24.26 (4.7)	527 (0.37, 0.56)
B2	**Ir-Ge** (6 wt%)	4.1	48566 (14.7)	13.31 (4.7)	48.25 (4.7)	33.89 (4.3)	527 (0.37, 0.56)
B3	**Ir-Ge** (8 wt%)	3.9	48567 (14.1)	13.36 (4.7)	48.44 (4.7)	32.56 (4.3)	527 (0.37, 0.56)
B4	**Ir-Ge** (10 wt%)	4.1	48460 (13.5)	12.84 (4.7)	46.57 (4.7)	30.16 (4.5)	527 (0.37, 0.56)
C1	**Ir-N** (4 wt%)	3.5	48231 (12.7)	10.13 (4.9)	44.20 (4.9)	30.66 (4.3)	531 (0.32, 0.66)
C2	**Ir-N** (6 wt%)	3.3	48444 (12.9)	13.13 (4.3)	57.27 (4.3)	44.21 (3.9)	531 (0.32, 0.66)
C3	**Ir-N** (8 wt%)	3.3	48576 (12.3)	13.93 (4.1)	60.76 (4.1)	49.05 (3.5)	531 (0.32, 0.66)
C4	**Ir-N** (10 wt%)	3.3	48348 (12.5)	10.81 (4.7)	47.16 (4.7)	34.48 (3.7)	531 (0.32, 0.66)
D1	**Ir-PO** (4 wt%)	3.7	37001 (13.9)	8.84 (4.1)	31.24 (4.1)	25.04 (3.9)	528 (0.37, 0.57)
D2	**Ir-PO** (6 wt%)	3.5	47994 (13.5)	9.67 (4.7)	34.23 (4.7)	23.64 (4.3)	531 (0.39, 0.58)
D3	**Ir-PO** (8 wt%)	3.5	47969 (13.7)	9.50 (6.7)	33.57 (6.7)	24.32 (4.1)	532 (0.40, 0.58)
D4	**Ir-PO** (10 wt%)	3.5	47328 (13.7)	7.93 (7.9)	28.02 (4.7)	15.88 (7.9)	532 (0.40, 0.57)
E1	**Ir-O** (4 wt%)	3.7	31567 (14.3)	6.20 (7.7)	18.48 (7.7)	8.64 (5.7)	496 (0.20, 0.60)
E2	**Ir-O** (6 wt%)	3.7	28256 (14.1)	7.19 (4.9)	21.42 (4.9)	14.66 (4.5)	496 (0.20, 0.60)
E3	**Ir-O** (8 wt%)	3.9	38561 (14.7)	8.92 (5.1)	26.59 (5.1)	18.10 (4.5)	4496 (0.20, 0.60)
E4	**Ir-O** (10 wt%)	3.9	38561 (14.7)	8.22 (5.3)	24.50 (5.3)	16.64 (4.3)	496 (0.20, 0.60)
F1	**Ir-S** (4 wt%)	3.5	45393 (12.3)	9.28 (4.5)	34.17 (4.5)	23.88 (4.3)	518 (0.35, 0.61)
F2	**Ir-S** (6 wt%)	3.5	48359 (12.3)	11.05 (4.1)	40.70 (4.1)	31.17 (4.1)	519 (0.34, 0.62)
F3	**Ir-S** (8 wt%)	3.5	48318 (12.1)	12.46 (4.3)	45.90 (4.3)	35.01 (4.1)	520 (0.35, 0.62)
F4	**Ir-S** (10 wt%)	3.3	48192 (11.9)	12.36 (4.5)	45.54 (4.5)	32.86 (4.3)	521 (0.35, 0.61)
G1	**Ir-SO$_2$** (4 wt%)	3.7	48574 (11.9)	9.81 (5.3)	36.50 (5.3)	23.25 (4.7)	529 (0.37, 0.59)
G2	**Ir-SO$_2$** (6 wt%)	3.5	48185 (12.3)	10.12 (4.9)	37.63 (4.9)	26.05 (4.3)	529 (0.37, 0.59)
G3	**Ir-SO$_2$** (8 wt%)	3.3	48501 (11.7)	9.14 (5.1)	33.99 (5.1)	22.35 (4.5)	529 (0.37, 0.59)
G4	**Ir-SO$_2$** (10 wt%)	3.3	48582 (12.3)	7.86 (5.1)	29.23 (5.1)	18.60 (4.3)	529 (0.37, 0.59)
R1[d]	**Ir(ppy)$_3$** (6 mol%)	–	–	10.0	–	32.0 (3.5)	–
R2[e]	**Ir(ppy)$_3$** (6 wt%)	3.1	~70000 (11.0)	8.0	28.0	31.0 (3.0)	510 (0.27, 0.63)
R3[f]	**Ir(ppy)$_3$** (7 wt%)	–	–	9.0, 15.4	–	40.0	–

[a] Some representive EL data of $Ir(ppy)_3$ with a similar device structure reported in the literature are also included. [b] Maximum values of the devices. Values in parentheses are the voltages at which they were obtained. [c] Values were collected at 8 V and CIE coordinates (x, y) are shown in parentheses. [d] Results reported in Ref. [9a] with a similar device structure. [e] Results reported in Ref. [3b] with a similar device structure. [f] Results reported in Ref. [9b], and the higher η_{ext} and η_p values are obtained from the optimized device structure by using the host showing electron-transporting properties. The lower η_{ext} value corresponds to the data from the device with CBP as the host.

and L_{max} of 47994 cd m^{-2} at 13.5 V. Device G2 (6 wt% **Ir-SO$_2$**), which exhibits η_{ext} of 10.1%, η_L of 37.6 cd A^{-1}, η_p of 26.1 Lm W^{-1}, and L_{max} of 48185 cd m^{-2} at 12.3 V, slightly outperforms that of device D2. To the best of our knowledge, devices D1–D4 and G1–G4 provide the first examples of green-emitting PHOLEDs with EI/ET properties. Representative current-density–voltage–luminance (J-V-L) characteristics and the efficiency versus current-density relationship of devices A2, C3, F3, and G2 are shown in Figure 7 (also see Figures S4–S10 in the Supporting Information). Remarkably, the efficiency roll off at high current densities is not very severe in most of our devices, implying that the triplet–triplet annihilation effect is not very significant. This desirable character of the PHOLEDs might be attributed to the short τ_p of the phosphors and their sterically congested structure, which effectively blocks the non-emissive pathways provided by various intermolecular excited-state interactions. Notably, other factors such as carrier recombination and emission width would also control the roll-off characteristics.[20]

There are many reports about high-efficiency $Ir(ppy)_3$-based green-emitting PHOLEDs. Those with a similar configuration as our devices only show peak efficiencies η_{ext} of 8.0%, η_L of 28.0 cd A^{-1}, and η_p of 31.0 Lm W^{-1}.[3b] After $Ir(ppy)_3$ is doped into an electron-transporting host, the power efficiency of the PHOLEDs can reach 40.0 Lm W^{-1}.[9b] When new starburst perfluorinated phenylenes and 4,4′,4″-tris(*N*-carbazolyl)triphenylamine were employed as both the exciton-blocking and host materials, respectively, the maximum efficiencies of the $Ir(ppy)_3$-based PHOLEDs can reach η_{ext} of 19.2% and η_p of 70 Lm W^{-1}.[9a] However, the high performance of the PHOLEDs in these

 © 2008 Wiley-VCH Verlag GmbH & Co. KGaA, Weinheim

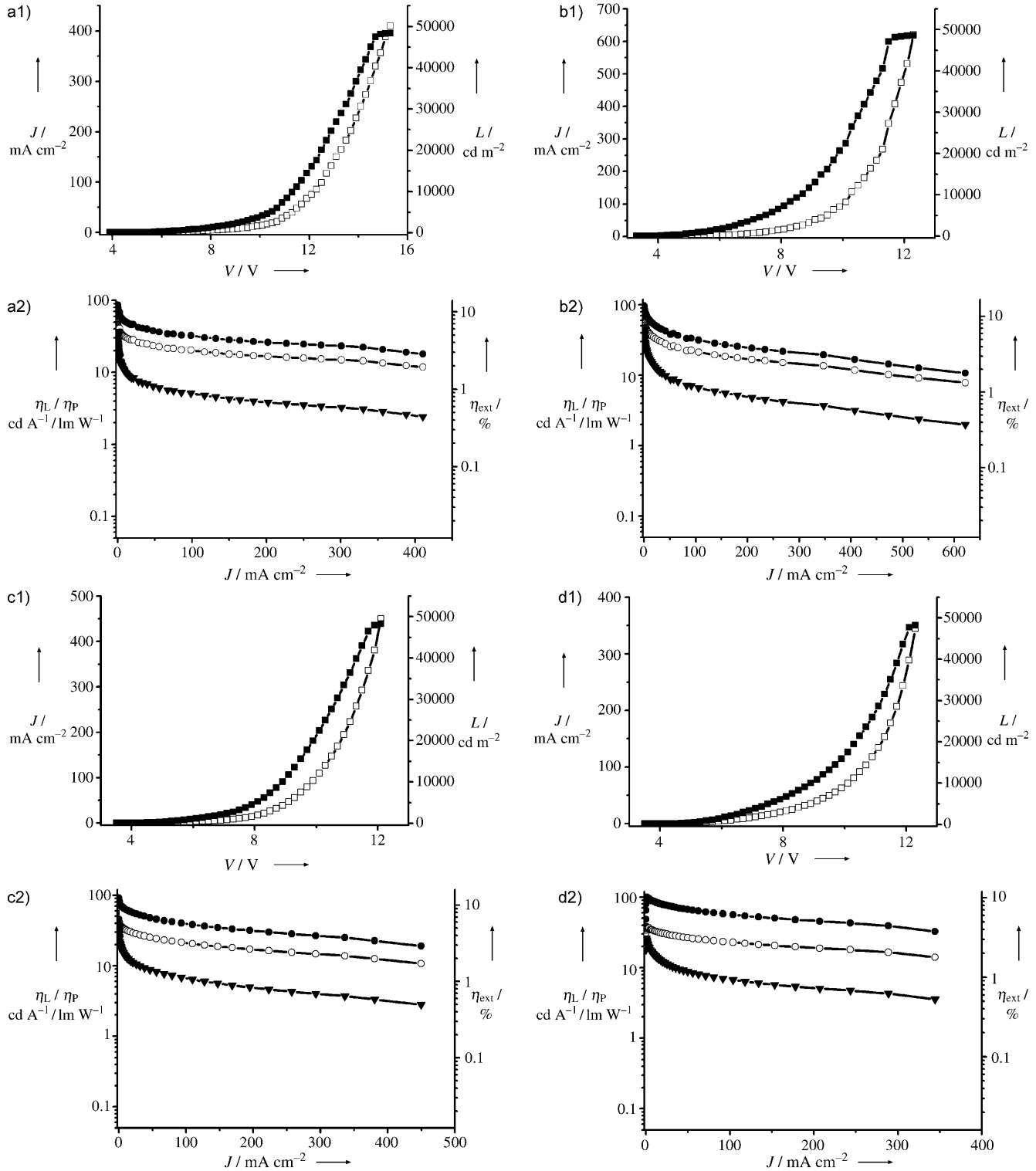

Figure 7. The *J*–*V*–*L* curves and the efficiency versus current-density relationship for a) Device A2, b) Device C3, c) Device F3, d) Device G2. ■: *L*, □: *J*, ●: η_{ext}, ○: η_L, ▼: η_p.

cases came mainly from the advance of new exciton-blocking and host materials, whereas the PHOLEDs with BCP as the exciton-block material and CBP as the host showed the peak efficiencies with η_{ext} of approximately 10.0% and η_p of approximately 32.0 Lm W^{-1}.[9a] It can be seen that most of our devices that use Ir^{III} dopants with effective charge-carrier-trapping moieties, show much higher EL efficiencies than state-of-the-art devices under the same device configuration.

 © 2008 Wiley-VCH Verlag GmbH & Co. KGaA, Weinheim

This is in line with the reported results for the better EL performance of [Ir(ppy-NPh_2)$_2$(acac)] over [Ir(ppy)$_2$(acac)] owing to the attachment of the hole-trapping NPh_2 moiety to the parent [Ir(ppy)$_2$(acac)].[11c] This indicates the great potential of our robust green phosphors in the realization of monochromatic and white-light OLEDs.

Conclusions

To investigate an effective method for carrier injection into and charge trapping in the metal phosphor of organic electrophosphorescent devices, we have synthesized a new class of green-emitting iridium(III) electrophosphors that exhibit highly efficient phosphorescence through a rational design with main-group 14–16 main-group moieties as the pendant antennas. This new strategy would confer the desirable HI/HT or EI/ET character to these phosphorescent metal complexes. Owing to their unique charge-injection and transport properties, they are promising emitters for robust EL devices with maximum EL performance at η_{ext} of 13.9%, η_L of 60.8 cd A^{-1}, and η_p of 49.1 Lm W^{-1}, which is superior to that of Ir(ppy)$_3$. These metalated materials should have great potential to excel in the development of green-emitting PHOLEDs and the relevance of these green phosphors in WOLEDs is under intensive study. Further device-optimization studies are ongoing in our laboratories.

Experimental Section

General Information

All reactions were performed under a nitrogen atmosphere. Solvents were carefully dried and distilled from appropriate drying agents prior to use. Commercially available reagents were used without further purification unless otherwise stated. All reactions were monitored by TLC with Merck pre-coated glass plates. Flash column chromatography and preparative TLC were carried out by using silica gel from Merck (230–400 mesh). Fast atom bombardment (FAB) mass spectra were recorded on a Finnigan MAT SSQ710 system. Proton, $^{13}C\{^1H\}$ and $^{31}P\{^1H\}$ NMR spectra were measured in $CDCl_3$ on a Varian Inova 400 MHz or JEOL GX270 FT-NMR spectrometer and chemical shifts are quoted relative to tetramethylsilane.

Physical Measurements

UV/Vis spectra were obtained on an HP-8453 diode array spectrophotometer. The photoluminescent properties of the compounds were examined by using a Photon Technology International (PTI) Fluorescence QuantaMaster Series QM1 system. The phosphorescence quantum yields were determined in CH_2Cl_2 solutions at 293 K against *fac*-Ir(ppy)$_3$ standard ($\Phi_P = 0.40$).[21] For phosphorescence-lifetime measurements, samples were prepared in CH_2Cl_2 solutions and were degassed through at least three freeze–pump–thaw cycles on a grease-free, turbo-pumped, high-vacuum line to a pressure of approximately 5×10^{-5} Torr in each cycle. Phosphorescence lifetimes were measured in degassed CH_2Cl_2 with a Lecroy Wave Runner 6100 digital oscilloscope using the third harmonic of a Nd:YAG laser ($\lambda = 355$ nm, pulse width = 8 ns) as the excitation source (Spectra-Physics Quantum-Ray). The decay curves were analyzed by using a Marquardt-based nonlinear least-squares fitting routine and were shown to follow a single-exponential function in each case according to $I = I_0 + A\exp(-t/\tau)$. The associated error with measured lifetimes is ±5%. Electrochemical measurements were made using a Princeton Applied Research model 273 A potentiostat at a scan rate of 100 mV s^{-1}. A conventional three-electrode configuration consisting of a glassy carbon working electrode, a Pt-sheet counter electrode, and a Pt-wire reference electrode was used. The supporting electrolyte was 0.1 M $[Bu_4N]PF_6$ in THF. Ferrocene was added as a calibrant after each set of measurements, and all potentials reported were quoted with reference to the ferrocene–ferrocenium (Fc/Fc^+) couple (taken as $E_{1/2} = +0.27$ V relative to the reference electrode). The oxidation (E_{ox}) and reduction (E_{red}) potentials were used to determine the HOMO and LUMO energy levels by using the equations $E_{HOMO} = -(E_{ox}+4.8)$ eV and $E_{LUMO} = -(E_{red}+4.8)$ eV, which were calculated by using the internal-standard ferrocene value of −4.8 eV with respect to the vacuum level.[22] Thermal analyses were performed with Perkin–Elmer Pyris Diamond DSC and Perkin–Elmer TGA6 thermal analyzers at a scan rate of 20 °C min^{-1}.

General Procedure for the Synthesis of Iridium Complexes

Under a N_2 atmosphere, each appropriate cyclometalating ligand and approximately 0.25 equiv of [Ir(acac)$_3$] were heated to 230 °C in glycerol for 18 h. Then the reaction mixture was cooled to room temperature and water was added. After extraction with CH_2Cl_2, the organic phase was dried over $MgSO_4$ and the solvent was then removed under reduced pressure. The residue was obtained as a crude product, which was chromatographed on a silica column by using an appropriate eluent to produce a pure sample of each of the title iridium complexes in approximately 15–20% overall yields after solvent evaporation and drying.

Ir-Si: Yield: 20%; yellow solid. ^1H NMR (270 MHz, $CDCl_3$): $\delta = 7.77$ (d, $J = 8.1$ Hz, 3H, Ar), 7.62 (d, $J = 5.4$ Hz, 3H, Ar), 7.58–7.52 (m, 3H, Ar), 7.33 (d, $J = 7.8$ Hz, 3H, Ar), 7.21–7.13 (m, 30H, Ar), 7.01–6.95 (m, 18H, Ar), 6.82–6.74 ppm (m, 6H, Ar); ^{13}C NMR (67.5 MHz, $CDCl_3$): $\delta =$ 166.61, 159.34, 147.53, 144.64, 144.55, 136.15, 135.61, 135.18, 134.07, 128.66, 127.73, 127.38, 123.01, 121.84, 118.80 ppm; FAB-MS (*m*/*z*): 1429 $[M]^+$; elemental analysis calcd (%) for $C_{87}H_{66}IrN_3Si_3$: C 73.07, H 4.65, N 2.94; found: C 72.96, H 4.42, N 2.78.

Ir-Ge: Yield: 18%; pale yellow solid. ^1H NMR (400 MHz, $CDCl_3$): $\delta =$ 7.77 (d, $J = 8.1$ Hz, 3H, Ar), 7.61 (d, $J = 5.1$ Hz, 3H, Ar), 7.55–7.49 (m, 3H, Ar), 7.38 (d, $J = 7.6$ Hz, 3H, Ar), 7.19–7.08 (m, 30H, Ar), 7.05–6.97 (m, 18H, Ar), 6.81–6.75 ppm (m, 6H, Ar); ^{13}C NMR (67.5 MHz, $CDCl_3$): $\delta = 166.47$, 159.93, 147.33, 143.99, 143.45, 137.03, 136.40, 135.56, 135.07, 128.11, 127.67, 126.52, 123.35, 121.73, 118.64 ppm (Ar); FAB-MS (*m*/*z*): 1564 $[M]^+$; elemental analysis calcd (%) for $C_{87}H_{66}IrN_3Ge_3$: C 66.83, H 4.25, N 2.69; found: C 66.67, H 4.37, N 2.75.

Ir-N: Yield: 20%; orange-yellow solid. ^1H NMR (400 MHz, $CDCl_3$): $\delta =$ 7.66 (d, $J = 7.6$ Hz, 3H, Ar), 7.53–7.52 (m, 6H, Ar), 7.25 (d, $J = 10.0$ Hz, 3H, Ar), 7.09–7.05 (m, 12H, Ar), 6.87–6.74 (m, 21H, Ar), 6.56 (s, 3H, Ar), 6.23 ppm (d, $J = 8.0$ Hz, 3H, Ar); ^{13}C NMR (100.6 MHz, $CDCl_3$): $\delta = 166.22$, 161.84, 148.22, 147.60, 147.21, 137.52, 135.42, 130.15, 128.56, 124.74, 124.49, 122.14, 120.49, 117.72, 114.55 ppm (Ar); FAB-MS (*m*/*z*): 1156 $[M]^+$; elemental analysis calcd (%) for $C_{69}H_{51}IrN_6$: C 71.67, H 4.45, N 7.27; found: C 71.58, H 4.35, N 7.18.

Ir-PO: Yield: 15%; yellow solid. ^1H NMR (400 MHz, $CDCl_3$): $\delta = 7.78$ (d, $J = 8.0$ Hz, 3H, Ar), 7.68–7.64 (m, 3H, Ar), 7.58–7.56 (m, 3H, Ar), 7.44–7.30 (m, 18H, Ar), 7.17–7.01 (m, 18H, Ar), 6.93–6.90 (m, 3H, Ar), 6.55 (dd, $J = 12.8$, 1.6 Hz, 2H, Ar); ^{31}P NMR (161.9 MHz, $CDCl_3$): $\delta =$ 30.67 ppm; FAB-MS (*m*/*z*): 1255 $[M]^+$; elemental analysis calcd (%) for $C_{69}H_{51}IrN_3O_3P_3$: C 66.02, H 4.10, N 3.35; found: C 65.94, H 4.12, N 3.20.

Ir-O: Yield: 16%; yellow solid. ^1H NMR (400 MHz, $CDCl_3$): $\delta = 7.76$ (d, $J = 8.4$ Hz, 3H, Ar), 7.58–7.51 (m, 9H, Ar), 7.16–7.12 (m, 6H, Ar), 6.95 (t, $J = 7.4$ Hz, 3H, Ar), 6.85–6.80 (m, 9H, Ar), 6.55 (d, $J = 2.4$ Hz, 3H, Ar), 6.42 ppm (dd, $J = 8.4$, 2.8 Hz, 3H, Ar); ^{13}C NMR (100.6 MHz, $CDCl_3$): $\delta = 165.97$, 163.12, 158.02, 157.32, 147.05, 139.12, 135.96, 129.25, 126.33, 125.35, 122.29, 121.26, 118.66, 118.45, 110.73 ppm (Ar); FAB-MS (*m*/*z*): 931 $[M]^+$; elemental analysis calcd (%) for $C_{51}H_{36}IrN_3O_3$: C 65.79, H 3.90, N 4.51; found: C 65.65, H 3.82, N 4.60.

Ir-S: Yield: 12%; yellow solid. ^1H NMR (400 MHz, $CDCl_3$): $\delta = 7.76$ (d, $J = 8.0$ Hz, 3H, Ar), 7.59–7.55 (m, 3H, Ar), 7.48–7.46 (m, 3H, Ar), 7.45 (d, $J = 8.0$ Hz, 3H, Ar), 7.19–7.09 (m, 15H, Ar), 6.87–6.83 (m, 3H, Ar), 6.80 (d, $J = 1.6$ Hz, 3H, Ar), 6.76 ppm (dd, $J = 8.0$, 2.0 Hz, 3H, Ar);

 © 2008 Wiley-VCH Verlag GmbH & Co. KGaA, Weinheim

^{13}C NMR (100.6 MHz, $CDCl_3$): δ = 165.94, 160.79, 157.06, 142.47, 138.80, 136.79, 136.39, 136.06, 130.57, 128.80, 126.29, 124.56, 122.55, 121.87, 118.88 ppm (Ar); FAB-MS (*m*/*z*): 979 $[M]^+$; elemental analysis calcd (%) for $C_{51}H_{36}IrN_3S_3$: C 62.55, H 3.71, N 4.29; found: C 62.51, H 3.80, N 4.32.

Ir-SO$_2$: Yield: 10%; yellow solid. ^{1}H NMR (400 MHz, acetone/d_6): δ = 8.23 (d, J = 8.0 Hz, 3H, Ar), 7.94 (d, J = 8.0 Hz, 3H, Ar), 7.90–7.86 (m, 3H, Ar), 7.70–7.68 (m, 3H, Ar), 7.65–7.62 (m, 6H, Ar), 7.55–7.45 (m, 9H, Ar), 7.40 (dd, J = 8.0, 2.0 Hz, 3H, Ar), 7.27 (d, J = 2.0 Hz, 3H, Ar), 7.21–7.17 ppm (m, 3H, Ar); FAB-MS (*m*/*z*): 1075 $[M]^+$; elemental analysis calcd (%) for $C_{51}H_{36}IrN_3O_6S_3$: C 56.97, H 3.37, N 3.91; found: C 56.88, H 3.47, N 3.85.

X-ray Crystallography

X-ray diffraction data were collected at 293 K by using graphite-monochromated $Mo_{K\alpha}$ radiation (λ = 0.71073 Å) on a Bruker Axs SMART 1000 CCD diffractometer. The collected frames were processed with the software SAINT+[23] and an absorption correction (SADABS)[24] was applied to the collected reflections. The structure was solved by the Direct methods (SHELXTL)[25] in conjunction with standard-difference Fourier techniques and subsequently refined by full-matrix least-squares analyses on F^2. Hydrogen atoms were generated in their idealized positions and all non-hydrogen atoms were refined anisotropically. CCDC 672369, 672370, and 672371 contain the supplementary crystallographic data for this paper. These data can be obtained free of charge from The Cambridge Crystallographic Data Centre via www.ccdc.cam.ac.uk/data_request/cif. Crystal data for **Ir-SO$_2$**: $C_{54}H_{42}N_3O_7S_3Ir$ M_w = 1133.29, monoclinic, space group $P\bar{1}$, a = 12.5874(8), b = 12.8280(8), c = 16.459(1) Å, α = 96.183(1), β = 107.872(1), γ = 107.236(1)°, V = 2357.4(3) Å^3, Z = 2, ρ_{calcd} = 1.597 mg m^{-3}, $\mu(Mo_{K\alpha})$ = 3.023 mm^{-1}, $F(000)$ = 1136. 13997 Reflections measured of which 10224 were unique (R_{int} = 0.0138). Final R_1 = 0.0235 and wR_2 = 0.0575 for 9384 observed reflections with $I > 2\sigma(I)$.

OLED Fabrication and Measurements

The pre-cleaned ITO glass substrates were treated with ozone for 20 min. Then, a 40-nm-thick NPB film was deposited on the ITO glass substrates. The iridium phosphor and CBP host were co-evaporated to form a 20-nm emitting layer. Successively, BCP, Alq_3, LiF, and Al were evaporated at a base pressure of less than 10^{-6} Torr. The EL spectra and CIE (commission internationale de l'éclairage) coordinates were measured with a PR650 Spectra colorimeter. The J–V–L curves of the devices were recorded by using a Keithley 2400/2000 source meter, and the luminance was measured by using a PR650 SpectraScan spectrometer. All of the experiments and measurements were carried out at room temperature under ambient conditions.

Computational Details

Density functional theory (DFT) calculations at the B3LYP level were performed based on experimental geometries from the X-ray diffraction data. The basis set used for C, H, N, and O atoms was 6-31G while the effective core potentials with a LanL2DZ basis set were employed for S and Ir atoms.[26] Polarization functions were added for S (ζ_d(S) = 0.421). All calculations were carried out by using the Gaussian 03 program.[27] Mulliken population analyses were done by using MullPop.[28] Frontier molecular orbitals obtained from the DFT calculations were plotted by using the Molden 3.7 program written by Schaftenaar.[29]

[1] a) C. W. Tang, S. A. VanSlyke, *Appl. Phys. Lett.* **1987**, *51*, 913; b) S. C. Stinson, *Chem. Eng. News* **2000**, *78*, 22; c) W. E. Howard, *Sci. Am.* **2004**, *290*, 76; d) B. Johnstone, *Technol. Rev.* **2001**, *104*, 80; e) O. Gelson, *Opt. Laser Eur.* **2003**, *107*, 33.

[2] a) D. Liu, M. Fina, Z. Y. Chen, X. B. Chen, G. Liu, S. Johnson, S. S. Mao, *Appl. Phys. Lett.* **1999**, *91*, 093514; b) T. Karatsu, R. Hazuku, M. Asuke, A. Nishigaki, S. Yagai, Y. Suzuri, H. Kita, A. Kitamura, *Org. Electron.* **2007**, *8*, 357; c) H. R. Rathnayake, A. Cirpan, Z. Delen, P. M. Lahti, F. E. Karasz, *Adv. Funct. Mater.* **2007**, *17*, 115; d) C.-T. Chen, *Chem. Mater.* **2004**, *16*, 4389; e) K. T. Kamtekar, C. S. Wang, S. Bettington, A. S. Batsanov, J. H. Ahn, M. Rabinal, M. C. Petty, *J. Mater. Chem.* **2006**, *16*, 3823; f) K.-T. Wong, Y.-M. Chen, Y.-T. Lin, H.-C. Su, C.-C. Wu, *Org. Lett.* **2005**, *7*, 5361.

[3] a) M. A. Baldo, D. F. O'Brien, Y. You, A. Shoustikov, S. Sibley, M. E. Thompson, S. R. Forrest, *Nature* **1998**, *395*, 151; b) M. A. Baldo, S. Lemansky, P. E. Burrows, M. E. Thompson, S. R. Forrest, *Appl. Phys. Lett.* **1999**, *75*, 4; c) M. A. Baldo, M. E. Thompson, S. R. Forrest, *Nature* **2000**, *403*, 750; d) A. Kohler, J. S. Wilson, R. H. Friend, *Adv. Mater.* **2002**, *14*, 701; e) S. R. Forrest, *Org. Electron.* **2003**, *4*, 45; f) W.-S. Huang, J.-T. Lin, C.-H. Chien, Y.-T. Tao, S.-S. Sun, Y.-S. Wen, *Chem. Mater.* **2004**, *16*, 2480; g) S. Lamansky, P. Djurovich, D. Murphy, F. Abdel-Razzaq, H.-E. Lee, C. Adachi, P. E. Burrows, S. R. Forrest, M. E. Thompson, *J. Am. Chem. Soc.* **2001**, *123*, 4304; h) P. L. Burn, S.-C. Lo, I. D. W. Samuel, *Adv. Mater.* **2007**, *19*, 1675; i) B. M. W. Langeveld, U. S. Schubert, *Adv. Mater.* **2005**, *17*, 1109; j) P.-T. Chou, Y. Chi, *Chem. Eur. J.* **2007**, *13*, 380; k) Y. Chi, P.-T. Chou, *Chem. Soc. Rev.* **2007**, *36*, 1421.

[4] a) B. W. D'Andrade, M. E. Thompson, S. R. Forrest, *Adv. Mater.* **2002**, *14*, 147; b) S. Tokito, T. Iijimia, T. Tsuzuki, F. Sato, *Appl. Phys. Lett.* **2003**, *83*, 2459; c) M. Hack, J. J. Brown, *Inf. Disp.* **2004**, *20*, 12; d) J. R. Sheats, *J. Mater. Res.* **2004**, *19*, 1974; e) B. W. D'Andrade, R. J. Holmes, S. R. Forrest, *Adv. Mater.* **2004**, *16*, 624; f) A. Misra, P. Kumar, M. N. Kamalasanan, S. Chandra, *Semicond. Sci. Technol.* **2006**, *21*, R35; g) B. W. D'Andrade, S. R. Forrest, *Adv. Mater.* **2004**, *16*, 1585; h) A. J. Heeger, *Solid State Commun.* **1998**, *107*, 673; i) X. Niu, L. Ma, B. Yao, J. Ding, G. Tu, Z. Xie, L. Wang, *Appl. Phys. Lett.* **2006**, *89*, 213508; j) H. Kanno, Y. Sun, S. R. Forrest, *Appl. Phys. Lett.* **2005**, *86*, 263502; k) T. Fuhrmann, J. Salbeck, *MRS Bull.* **2003**, *28*, 354; l) R. J. Holmes, B. W. D'Andrade, X. Ren, J. Li, M. E. Thompson, S. R. Forrest, *Appl. Phys. Lett.* **2003**, *83*, 3818; m) V. Adamovich, J. Brooks, A. Tamayo, A. M. Alexander, P. I. Djurovich, B. W. D'Andrade, C. Adachi, S. R. Forrest, M. E. Thompson, *New J. Chem.* **2002**, *26*, 1171; n) J. Liu, Q. Zhou, Y. Cheng, Y. Geng, L. Wang, D. Ma, X. Jing, F. Wang, *Adv. Funct. Mater.* **2006**, *16*, 957; o) J. X. Jiang, Y. H. Xu, W. Yang, R. Guan, Z. Q. Liu, H. Y. Zhen, Y. Cao, *Adv. Mater.* **2006**, *18*, 1769..

[5] X.-M. Yu, H.-S. Kwok, W.-Y. Wong, G.-J. Zhou, *Chem. Mater.* **2006**, *18*, 5097.

[6] a) G. Cheng, Y. Zhang, Y. Zhao, Y. Lin, C. Ruan, S. Liu, T. Fei, Y. Ma, Y. Cheng, *Appl. Phys. Lett.* **2006**, *89*, 043504; b) Y. Shao, Y. Yang, *Appl. Phys. Lett.* **2005**, *86*, 073510.

[7] a) P. Coppo, E. A. Plummer, L. De Cola, *Chem. Commun.* **2004**, 1774; b) S.-C. Lo, C. P. Shipley, R. N. Bera, R. E. Harding, A. R. Cowley, P. L. Burn, I. D. W. Samuel, *Chem. Mater.* **2006**, *18*, 5119; c) C. Adachi, R. C. Kwong, P. Djurovich, V. Adamovich, M. A. Baldo, M. E. Thompson, S. R. Forrest, *Appl. Phys. Lett.* **2001**, *79*, 2082; d) S.-J. Yeh, M.-F. Wu, C.-T. Chen, Y.-H. Song, Y. Chi, M.-H. Ho, S.-F. Hsu, C. H. Chen, *Adv. Mater.* **2005**, *17*, 285; e) C.-H. Yang, Y.-M. Cheng, Y. Chi, C.-J. Hsu, F.-C. Fang, K.-T. Wong, P.-T. Chou, C.-H. Chang, M.-H. Tsai, C.-C. Wu, *Angew. Chem.* **2007**, *119*, 2470; *Angew. Chem. Int. Ed.* **2007**, *46*, 2418.

[8] a) C. Jiang, W. Yang, J. Peng, S. Xiao, Y. Cao, *Adv. Mater.* **2004**, *16*, 537; b) J.-P. Duan, P.-P. Sun, C.-H. Cheng, *Adv. Mater.* **2003**, *15*, 224; c) Y.-J. Su, H.-L. Huang, C.-L. Li, C.-H. Chien, Y.-T. Tao, P.-T. Chou, S. Datta, R.-S. Liu, *Adv. Mater.* **2003**, *15*, 884; d) S. Okada, K. Okinaka, H. Iwawaki, M. Furugori, M. Hashimoto, T. Mukaide, J. Kamatani, S. Igawa, A. Tsuboyama, T. Takiguchi, K. Ueno, *Dalton Trans.* **2005**, 1583; e) W.-Y. Wong, G.-J. Zhou, X.-M. Yu, H.-S. Kwok, B.-Z. Tang, *Adv. Funct. Mater.* **2006**, *16*, 838; f) C.-L. Li, Y.-J. Su, Y.-T. Tao, P.-T. Chou, C.-H. Chien, C.-C. Cheng, R.-S. Liu, *Adv. Funct. Mater.* **2005**, *15*, 387.

[9] a) M. Ikai, S. Tokito, Y. Sakamoto, T. Suzuki, Y. Taga, *Appl. Phys. Lett.* **2001**, *79*, 156; b) C. Adachi, M. A. Baldo, S. T. Forrest, M. E. Thompson, *Appl. Phys. Lett.* **2000**, *77*, 904.

[10] a) S.-C. Lo, N. A. H. Male, J. P. J. Markham, S. W. Magennis, P. L. Burn, O. V. Salata, I. D. W. Samuel, *Adv. Mater.* **2002**, *14*, 975; b) W.-Y. Wong, C.-L. Ho, Z.-Q. Gao, B.-X. Mi, C.-H. Chen, K.-W. Cheah, Z. Lin, *Angew. Chem.* **2006**, *118*, 7964; *Angew. Chem. Int. Ed.* **2006**, *45*, 7800; c) J. P. J. Markham, I. D. W. Samuel, S.-C. Lo, P. L. Burn, M. Weiter, H. Bässler, *J. Appl. Phys.* **2004**, *95*, 438; d) T. D. Antho-

 © 2008 Wiley-VCH Verlag GmbH & Co. KGaA, Weinheim

poulos, M. J. Frampton, E. B. Namdas, P. L. Burn, I. D. W. Samuel, *Adv. Mater.* **2004**, *16*, 557; e) Z. Liu, M. Guan, Z. Bian, D. Nie, Z. Gong, Z. Li, C. Huang, *Adv. Funct. Mater.* **2006**, *16*, 1441; f) T. Tsuzuki, N. Shirasawa, T. Suzuki, S. Tokito, *Adv. Mater.* **2003**, *15*, 1455.

[11] a) J. Q. Ding, J. Gao, Y. X. Cheng, Z. Y. Xie, L. X. Wang, D. G. Ma, X. B. Jing, F. S. Wang, *Adv. Funct. Mater.* **2006**, *16*, 575; b) G. J. Zhou, W.-Y. Wong, B. Yao, Z. Y. Xie, L. X. Wang, *Angew. Chem.* **2007**, *119*, 1167; *Angew. Chem. Int. Ed.* **2007**, *46*, 1149; c) J. Nishida, H. Echizen, T. Iwata, Y. Yamashita, *Chem. Lett.* **2005**, 1378; d) K. Ono, M. Joho, K. Saito, M. Tomura, Y. Matsushita, S. Naka, H. Okada, H. Onnagawa, *Eur. J. Inorg. Chem.* **2006**, 3676; e) Y. You, C.-G. An, D.-S. Lee, J.-J. Kim, S. Y. Park, *J. Mater. Chem.* **2006**, *16*, 4706; f) G.-J. Zhou, C.-L. Ho, W.-Y. Wong, Q. Wang, D.-G. Ma, L.-X. Wang, Z.-Y. Lin, T. B. Marder, A. Beeby, *Adv. Funct. Mater.* **2008**, *18*, 499; g) G.-J. Zhou, W.-Y. Wong, B. Yao, Z. Xie, L. Wang, *J. Mater. Chem.* **2008**, *18*, 1799.

[12] K. Dedeian, P. I. Djurovich, F. O. Garces, G. Carlson, R. J. Watts, *Inorg. Chem.* **1991**, *30*, 1685.

[13] X.-M. Liu, J. Xu, X. Lu, C. He, *Org. Lett.* **2005**, *7*, 2829.

[14] M. H. Chisholm, N. J. Patmore, *Dalton Trans.* **2006**, 3164.

[15] a) Y. You, S. Y. Park, *J. Am. Chem. Soc.* **2005**, *127*, 12438; b) A. Tsuboyama, H. Iwawaki, M. Furugori, T. Mukaide, J. Kamatani, S. Igawa, T. Moriyama, S. Miura, T. Takiguchi, S. Okada, M. Hoshino, K. Ueno, *J. Am. Chem. Soc.* **2003**, *125*, 12971; c) S. Jung, Y. Kang, H.-S. Kim, Y.-H. Kim, C.-L. Lee, J.-J. Kim, S.-K. Lee, S.-K. Kwon, *Eur. J. Inorg. Chem.* **2004**, 3415; d) M. S. Lowry, W. R. Hudson, R. A. Pascal, Jr., S. Bernhard, *J. Am. Chem. Soc.* **2004**, *126*, 14129; e) M. S. Lowry, J. I. Goldsmith, J. D. Slinker, R. Rohl, R. A. Pascal, Jr., G. G. Malliaras, S. Bernhard, *Chem. Mater.* **2005**, *17*, 5712; f) V. A. Montes, R. Pohl, J. Shinar, P. Anzenbacher, Jr., *Chem. Eur. J.* **2006**, *12*, 4523; g) T. Sajoto, P. I. Djurovich, A. Tamayo, M. Yousufuddin, R. Bau, M. E. Thompson, *Inorg. Chem.* **2005**, *44*, 7992; h) C.-J. Chang, C.-H. Yang, K. Chen, Y. Chi, C.-F. Shu, M.-L. Ho, Y.-S. Yeh, P.-T. Chou, *Dalton Trans.* **2007**, 1881.

[16] a) P. A. Vecchi, A. B. Padmaperuma, H. Qiao, L. S. Sapochak, P. E. Burrows, *Org. Lett.* **2006**, *8*, 4211; b) A. B. Padmaperuma, L. S. Sapochak, P. E. Burrows, *Chem. Mater.* **2006**, *18*, 2389; c) P. E. Burrows, A. B. Padmaperuma, L. S. Sapochak, P. Djurovich, M. E. Thompson, *Appl. Phys. Lett.* **2006**, *88*, 183503.

[17] P. J. Hay, *J. Phys. Chem. A* **2002**, *106*, 1634.

[18] K. Dedeian, J. Shi, N. Shepherd, E. Forsythe, D. Morton, *Inorg. Chem.* **2005**, *44*, 4445.

[19] a) D.-H. Hwang, S. T. Kim, H. K. Shim, A. B. Holmes, S. C. Moratti, R. H. Friend, *Chem. Commun.* **1996**, 2241; b) B. S. Chuah, D.-H Hwang, S. T. Kim, S. C. Moratti, A. B. Holmes, J. C. De Mello, R. H. Friend, *Synth. Met.* **1997**, *91*, 279.

[20] a) M. A. Baldo, C. Adachi, S. R. Forrest, *Phys. Rev. B* **2000**, *62*, 10967; b) C. Adachi, M. A. Baldo, S. R. Forrest, *J. Appl. Phys.* **2000**, *87*, 8049.

[21] K. A. King, P. J. Spellane, R.-J. Watts, *J. Am. Chem. Soc.* **1985**, *107*, 1431.

[22] a) M. Thelakkat, H.-W. Schmidt, *Adv. Mater.* **1998**, *10*, 219; b) R. S. Ashraf, M. Shahid, E. Klemm, M. Al-Ibrahim, S. Sensfuss, *Macromol. Rapid Commun.* **2006**, *27*, 1454.

[23] SAINT+, version 6.02a, Bruker Analytical X-ray System, Inc., Madison, WI, **1998**.

[24] G. M. Sheldrick, SADABS, Empirical Absorption Correction Program, University of Göttingen, Göttingen (Germany), **1997**.

[25] G. M. Sheldrick, SHELXTL, Reference Manual, ver. 5.1, Madison, WI, **1997**.

[26] a) W. R. Wadt, P. J. Hay, *J. Chem. Phys.* **1985**, *82*, 284; b) P. J. Hay, W. R. Wadt, *J. Chem. Phys.* **1985**, *82*, 299.

[27] Gaussian 03 (Revision B05), M. J. Frisch, G. W. Trucks, H. B. Schlegel, G. E. Scuseria, M. A. Robb, J. R. Cheeseman, J. A. Montgomery, T. Vreven, Jr., K. N. Kudin, J. C. Burant, J. M. Millam, S. S. Iyengar, J. Tomasi, V. Barone, B. Mennucci, M. Cossi, G. Scalmani, N. Rega, G. A. Petersson, H. Nakatsuji, M. Hada, M. Ehara, K. Toyota, R. Fukuda, J. Hasegawa, M. Ishida, T. Nakajima, Y. Honda, O. Kitao, H. Nakai, M. Klene, X. Li, J. E. Knox, H. P. Hratchian, J. B. Cross, C. Adamo, J. Jaramillo, R. Gomperts, R. E. Stratmann, O. Yazyev, A. J. Austin, R. Cammi, C. Pomelli, J. W. Ochterski, P. Y. Ayala, K. Morokuma, G. A. Voth, P. Salvador, J. J. Dannenberg, V. G. Zakrzewski, S. Dapprich, A. D. Daniels, M. C. Strain, O. Farkas, D. K. Malick, A. D. Rabuck, K. Raghavachari, J. B. Foresman, J. V. Ortiz, Q. Cui, A. G. Baboul, S. Clifford, J. Cioslowski, B. B. Stefanov, G. Liu, A. Liashenko, P. Piskorz, I. Komaromi, R. L. Martin, D. J. Fox, T. Keith, M. A. Al-Laham, C. Y. Peng, A. Nanayakkara, M. Challacombe, P. M. W. Gill, B. Johnson, W. Chen, M. W. Wong, C. Gonzalez, J. A. Pople, Gaussian, Inc., Pittsburgh, PA, **2003**.

[28] MullPop, a program written by Reinaldo Pis Diez at the National University of La Plata, Argentina.

[29] G. Schaftenaar, Molden v3.7; CAOS/CAMM Center Nijmegen: Toernooiveld, Nijmegen, Netherlands, **2001**.

Received: March 5, 2008
Revised: April 24, 2008
Published online: July 9, 2008

 © 2008 Wiley-VCH Verlag GmbH & Co. KGaA, Weinheim